Received: 12 August 2021 | Revised: 21 October 2021 | Accepted: 9 November 2021

DOI: 10.1111/micc.12738

Microcirculation WILEY

ORIGINAL ARTICLE

Modeling acute and chronic vascular responses to a major arterial occlusion

Erin Zhao[1] | Jared Barber[1] | Chandan K. Sen[2] | Julia Arciero[1]

[1]Department of Mathematical Sciences, Indiana University – Purdue University Indianapolis, Indianapolis, Indiana, USA

[2]Indiana Center for Regenerative Medicine and Engineering, Department of Surgery, Indiana University School of Medicine, Indianapolis, Indiana, USA

Correspondence
Julia Arciero, Department of Mathematical Sciences, Indiana University – Purdue University Indianapolis, 402 N. Blackford St., LD 270D, Indianapolis, IN 46202, USA.
Email: jarciero@iupui.edu

Funding information
This work is supported by NSF DMS-1559745, NSF DMS-1654019, and NIH R01EY030851 (to JA) and NIH R01DK128845, R01DK125835, R01DK114718, and U01DK119090 (to CS)

Abstract

Objective: To incorporate chronic vascular adaptations into a mathematical model of the rat hindlimb to simulate flow restoration following total occlusion of the femoral artery.

Methods: A vascular wall mechanics model is used to simulate acute and chronic vascular adaptations in the collateral arteries and collateral-dependent arterioles of the rat hindlimb. On an acute timeframe, the vascular tone of collateral arteries and distal arterioles is determined by responses to pressure, shear stress, and metabolic demand. On a chronic timeframe, sustained dilation of arteries and arterioles induces outward vessel remodeling represented by increased passive vessel diameter (arteriogenesis), and low venous oxygen saturation levels induce the growth of new capillaries represented by increased capillary number (angiogenesis).

Results: The model predicts that flow compensation to an occlusion is enhanced primarily by arteriogenesis of the collateral arteries on a chronic time frame. Blood flow autoregulation is predicted to be disrupted and to occur for higher pressure values following femoral arterial occlusion.

Conclusions: Structural adaptation of the vasculature allows for increased blood flow to the collateral-dependent region after occlusion. Although flow is still below pre-occlusion levels, model predictions indicate that interventions which enhance collateral arteriogenesis would have the greatest potential for restoring flow.

KEYWORDS
angiogenesis, arteriogenesis, autoregulation, femoral arterial occlusion, mathematical model, rat hindlimb, structural adaptation

1 | INTRODUCTION

Peripheral arterial disease (PAD) is an atherosclerotic pathology that affects approximately 8–12 million individuals in the United States[1] and is characterized by either full or partial occlusion of an artery in the peripheral circulation. Occlusion of an artery prevents sufficient blood flow from reaching dependent tissue regions supplied by the artery, which can physically manifest as intermittent claudication or critical limb ischemia.[2] These symptoms can lead to increased mortality or a diminished quality of life if PAD is not diagnosed and treated effectively.[1] While surgery is the primary treatment for PAD, less invasive PAD treatments are needed. Developing less invasive treatment methods requires a thorough understanding of the effects of arterial occlusion on the surrounding vascular network, as well as knowledge of the intrinsic mechanisms that generate flow compensation without medical intervention.

Abbreviations: C, capillaries; CIA, central iliac artery; COL, collateral; EF, external iliac and femoral arteries; IIA, internal iliac artery; LA, large arterioles; LV, large venules; PAD, peripheral arterial disease; SA, small arterioles; SV, small venules; VEGF, vascular endothelial growth factor.

Collateral vessels are key players in flow compensation following a major arterial occlusion since they form redundant pathways that can redirect flow to circumnavigate the site of occlusion. When a major artery is occluded, blood pressure distal to the occlusion decreases significantly, leading to a pressure gradient across the collateral arteries that induces flow toward dependent tissue regions.[3] In the first week following ligation of the rat femoral artery, Unthank et al.[4] showed a profound impact on flow due to changes in the collateral resistance rather than the distal microcirculation.

The primary long-term adaptations that occur in response to ischemia are the remodeling and growth of arteries (arteriogenesis) and the growth of new capillaries (angiogenesis). Following femoral artery ligation in the rat hindlimb, Ziegler et al.[5] found that resting perfusion continued to improve for seven days post-occlusion and then plateaued at 65% of normal flow. Perfusion responses were studied immediately after acute occlusion of the femoral artery and 2 weeks after permanent femoral artery ligation. Greater perfusion deficits occurred with increased metabolic demand in both cases. However, the deficits were smaller for the case of femoral ligation, indicating improved compensatory responses on a chronic time scale. Twenty-one days after femoral artery ligation in mice, Chalothorn et al.[6] reported a 143% increase in the lumen diameters of collateral vessels and an 86% increase in gastrocnemius capillary density. Herzog et al.[7] observed that collateral vessels approximately doubled in diameter within 7 days of femoral artery occlusion in rats. Similarly, Prior et al.[8] observed structural enlargement of collateral vessels and increased flow through them. Their study concluded that a combination of structural and functional changes accounted for this enhanced flow, but it did not indicate the primary mechanisms generating such changes. The effects of vascular tone and structural adaptation on the compensatory response to occlusion have not been quantified, motivating the need for theoretical modeling.

Previous theoretical studies identified the primary role of collateral vessels in flow compensation following major arterial occlusion[9] and simulated vascular responses to occlusion on an acute time frame.[10] The study by Zhao et al.[10] included a mechanistic description of flow regulation but did not allow for structural adaptation, and thus blood flow compensation was limited. Pries et al.[11,12] developed a theoretical model to predict structural adaptation in the non-occluded rat mesentery. The model by Pries et al.[11,12] was adapted by Gruionu et al.[13] to investigate the effectiveness of arterial arcades in maintaining perfusion after arterial obstruction. The model predicted that the adaptation of arteriolar arcades into collateral flow pathways restored perfusion to 78% of normal flow, but the model did not consider vascular adaptations downstream of the collateral. A similar model was used to track structural changes in the diameter of the mouse gracilis artery after resection of one of its blood supplies and was extended to include the time-delayed effects of hypoxia and inflammation.[14] Although these models explored the mechanisms behind structural adaptation, the simulated diameters were assumed to be under conditions of maximal vasodilation and no vascular tone. Further modeling is needed to determine the relationship between vessel tone and structural adaptation and to study whether adaptations of distal vessels can enhance flow compensation.

Theoretical models have also been developed to simulate angiogenesis and its effects on oxygen delivery to tissue. Ji et al.[15] modeled both sprouting and splitting forms of angiogenesis to assess their impact on tissue hypoxia under conditions of high metabolic demand. Liu et al.[16] developed a multiscale model of activity-induced angiogenesis in rat skeletal muscle by combining models of blood flow, oxygen transport, and VEGF reaction-diffusion with an agent-based model of endothelial cells forming capillary sprouts. However, neither model considered the effects of angiogenesis following a major arterial occlusion.

Secomb et al.[17] conducted theoretical simulations combining angiogenesis and structural adaptation to describe patterns of vascular network formation in the rat mesentery. Coupling angiogenesis, structural adaptation, and pruning[17] within a single model yielded outcomes consistent with experimentally observed networks. Such modeling success suggests that an accurate depiction of long-term vascular responses to major arterial occlusion should combine structural adaptation and angiogenesis.

The present study couples an existing model of acute responses to femoral arterial occlusion in the rat hindlimb[10] with new model components accounting for the chronic responses of arteriogenesis and angiogenesis. The acute model is based on changes in vascular smooth muscle tone in response to local stimuli. Sustained vasodilation is assumed to lead to structural enlargement of the vessels (ie, arteriogenesis), and low levels of oxygenation in regions distal to the occlusion trigger an increase in capillary number (ie, angiogenesis). Incorporating vasomotor tone and structural adaptation in a single mathematical model allows for a more complete theoretical representation of changes in the vascular network following occlusion. Consistent with experimental observations, the model predicts that blood flow compensation in the region distal to occlusion is enhanced on the chronic time frame and that blood flow autoregulation is severely disrupted by arterial occlusion. Model predictions show that long-term responses ameliorate the disruption in tissue perfusion and autoregulation but do not fully restore the system to non-occluded flow levels.

2 | MATERIALS AND METHODS

In this study, a mathematical model is developed to predict the effect of acute and chronic vascular responses on flow to the rat hindlimb following a complete occlusion of the femoral artery. The vasculature of the rat hindlimb is modeled as an electrical circuit, in which compartments of vessels are represented by resistors, as depicted in Figure 1. Each resistor consists of a set of identical vessels (ie, same length and diameter) arranged in parallel. The closed black points in Figure 1 indicate the beginning and end of each

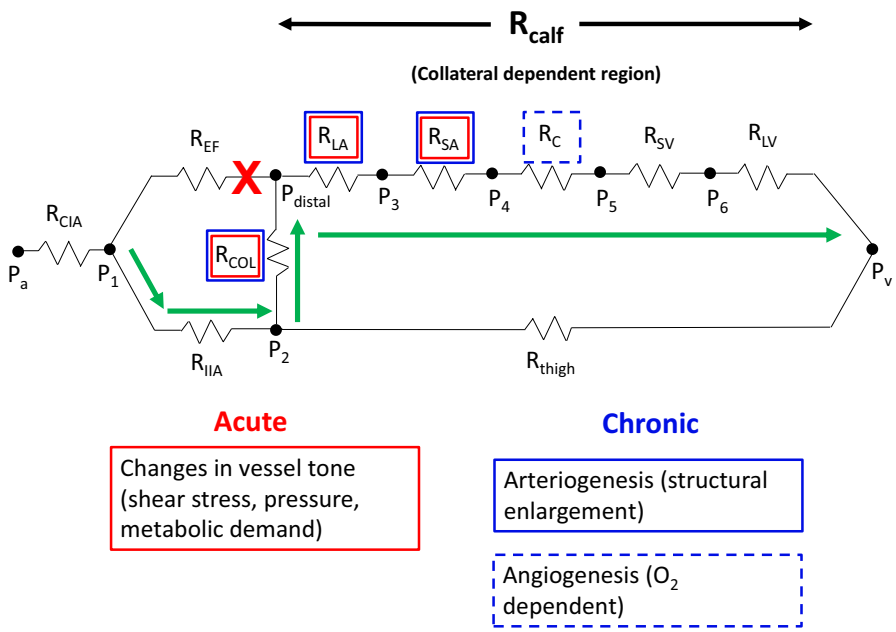

FIGURE 1 Circuit diagram of the rat hindlimb vasculature showing the location of nodes at which pressures are calculated and of resistors that represent compartments of each vessel type. The red X denotes the site of occlusion at the femoral artery, and green arrows depict the direction of flow through the collateral pathway. Compartments outlined in red are affected by acute responses, and compartments outlined in blue are affected by chronic responses (solid indicates arteriogenesis and dashed indicates angiogenesis). All other compartments are modeled using fixed resistances. A listing of the acute and chronic responses is also included below the circuit diagram

vessel compartment; pressure values are tracked at each of these points. The principles governing the flow of blood through the vascular network are analogous to Ohm's Law, which governs the flow of current in an electrical circuit. In particular, blood flow through vessels is proportional to the pressure drop along the vessel. Flow is conserved at each branch point, analogous to Kirchoff's laws. Flow enters the rat hindlimb through the central iliac artery (CIA), which divides into the external and femoral arteries (EF) along the top branch of the circuit and the internal iliac artery (IIA) along the bottom branch. A collateral artery compartment (COL) connects these two parallel branches of the circuit. In the absence of an occlusion, the EF branch primarily supplies blood to the calf region (R_{calf}) and the IIA primarily supplies flow to the thigh region (R_{thigh}). In the case of femoral arterial occlusion (red X in Figure 1), blood flow to the calf is dependent on flow through the collateral arteries, and thus the calf is termed the collateral-dependent region. The microcirculation of the calf is defined using five vessel compartments: large arterioles (LA), small arterioles (SA), capillaries (C), small venules (SV), and large venules (LV).

Figure 1 also provides a brief summary of which vessel compartments are affected by acute and/or chronic vascular responses in the mathematical model. The model includes vessel responses on an acute time frame to changes in pressure (myogenic response), flow (shear response), and oxygen saturation (metabolic response). These acute responses affect the diameters and vascular smooth muscle tone (activation) of the COL, LA, and SA compartments (indicated by red boxes in Figure 1). Two main types of chronic vascular responses are included in the model: structural enlargement of vessels (defined here as arteriogenesis; solid blue boxes in Figure 1) and new capillary growth (defined here as angiogenesis; dashed blue boxes in Figure 1).

2.1 | Model equations

2.1.1 | Acute response

A vessel wall mechanics model established previously[10,18,19] is adapted in this study to include both acute and chronic responses to a major arterial occlusion. Vessel constriction and dilation in the COL, LA, and SA are regulated by the degree of smooth muscle tone. These interactions are represented by differential equations for acute diameter (D_{acute}) and smooth muscle activation (A),

$$\begin{aligned}\frac{dD_{\text{acute},i}}{dt} &= \frac{1}{\tau_d}\frac{D_{c,i}}{T_{c,i}}\left(T_i - T_{\text{total},i}\right)\\ \frac{dA_i}{dt} &= \frac{1}{\tau_a}\left(A_{\text{total},i} - A_i\right),\end{aligned} \tag{1}$$

where $\tau_d = 1s$ and $\tau_a = 60s$ are diameter and activation time constants, D_c and T_c are the control values of diameter and tension, respectively (see control state section), and i = LA, SA, COL is the index that indicates the three vasoactive vessel compartments: large arterioles, small arterioles, and the collateral artery, respectively.

Total tension in a compartment is determined by the sum of passive tension and active tension (which is the product of smooth muscle activation and maximally active tension):

$$T_{\text{total},i} = T_{\text{pass},i} + A_i T^{\max}_{\text{act},i}. \tag{2}$$

Passive tension is modeled as an exponential function of vessel diameter, and maximally active tension is modeled as a Gaussian function, as in[18]:

$$T_{\text{pass},i} = C_{\text{pass},i}\exp\left(C'_{\text{pass},i}\left(\frac{D_{\text{acute},i}}{D_{0,\text{chronic},i}} - 1\right)\right). \tag{3}$$

$$T_{act,i}^{max} = C_{act,i}\exp\left(-\left(\frac{\frac{D_{acute,i}}{D_{0,chronic,i}} - C'_{act,i}}{C''_{act,i}}\right)^2\right). \quad (4)$$

Parameters values for $C_{pass,i}$, $C'_{pass,i}$, $C_{act,i}$, $C'_{act,i}$, and $C''_{act,i}$ in the COL, LA, and SA are taken from.[10] $D_{0,chronic,i}$ represents the passive diameter of the vessels under conditions of no smooth muscle tone and a pressure of 100 mmHg.

Total activation is a sigmoidal function of a stimulus for tone (S_{tone}), which is a linear combination of myogenic, shear, and metabolic responses:

$$A_{total,i} = \frac{1}{1+\exp\left(-S_{tone,i}\right)}. \quad (5)$$

$$S_{tone,i} = C_{myo,i}T_i - C_{shear,i}\tau_i - C_{meta,i}S_{CR,i} + C''_{tone,i}. \quad (6)$$

$C_{myo,i}$, $C_{shear,i}$, and $C_{meta,i}$ quantify the sensitivities of tone to the myogenic, shear, and metabolic responses, respectively, and $C''_{tone,i}$ accounts for other vascular responses and is determined by the control state assumptions (see Section 2.2); the values for these parameters are taken directly from Zhao et al.[10] All vessel wall mechanics model parameters are provided in Table 1.

The myogenic response is determined by circumferential wall tension $T_i = \frac{P_i D_i}{2}$ (Law of Laplace), where P_i is the pressure drop across the vessel wall and is equal to the intravascular pressure since the surrounding extravascular pressure is assumed negligible. The shear response is determined by the wall shear stress $\tau_i = \frac{32\mu_i Q_i}{\pi D_i^3}$, where Q_i is blood flow through the vessel and μ_i is the diameter-dependent viscosity calculated as in.[20]

The metabolic response depends on a conducted response (electrical) signal ($S_{CR,i}$) that is generated in the vessels according to the oxygen-dependent release of ATP (denoted by C and described in Equation 10) and conducted upstream along the vessel walls. The signal is assumed to decay exponentially in the upstream direction with a length constant of 1 cm. As in,[10] the total signal ($S_{CR,i}$) at the midpoint of each compartment (x_i) is given by the integral (sum) of ATP concentration multiplied by an exponential decay term:

$$S_{CR,i} = \begin{cases} 0.5\int_{x_{bif}}^{x_{end}} e^{-\frac{y-x_{bif}}{l_0}} C(y)\,dy + \int_{x_i}^{x_{bif}} e^{-\frac{y-x_i}{l_0}} C(y)\,dy & i = \text{COL} \\ \int_{x_i}^{x_{end}} e^{-\frac{y-x_i}{l_0}} C(y)\,dy & i = \text{LA, SA, C, SV, LV} \end{cases}. \quad (7)$$

When the signal reaches the branch bifurcation at P_{distal} (Figure 1), denoted by x_{bif} in Equation 7, the total signal is assumed to split evenly between the COL and the EF branches in both the occluded and non-occluded cases. Since the signal travels along the vessel wall, the lack of blood flow through the EF in the occluded case is assumed not to limit the splitting of the signal at the bifurcation point. Additionally, assessments using a diameter-dependent splitting rule showed that the model results do not depend significantly on this choice. Since the exact mechanism of signal splitting at bifurcations is unknown, an even split was assumed in this model. The signal in the COL is given by the sum of two integrals over different domains: (1) the signal from the calf multiplied by 0.5 to discount the half that goes to the EF and (2) the signal generated in the COL from x_{bif} to the given point x_i.

The delivery of oxygen to tissue is described using a Krogh cylinder model. In the Krogh model, each vessel runs along the central axis of a tissue cylinder and supplies only that tissue.[21] The total volume (V) of the vessels and their surrounding tissue cylinders is given by:

$$\begin{aligned} V &= \pi(n_{LA}L_{LA}\left(r_{LA}+d\right)^2 + n_{SA}L_{SA}\left(r_{SA}+d\right)^2 \\ &\quad + n_C L_C\left(r_C+d\right)^2 + n_{SV}L_{SV}r_{SV}^2 + n_{LV}L_{LV}r_{LV}^2, \end{aligned} \quad (8)$$

where n_i is the number of vessels in the compartment, L_i denotes the vessel length, r_i is the radius of the vessel, and d is the width of the tissue cylinders. Tissue width is not included in the SV and LV terms since oxygen exchange in the venules is neglected. No oxygen consumption is assumed in the COL compartment, and, regardless, the COL compartment is not included in Equation 8 since it is not located in the calf microcirculation. In the control state (see Section 2.2), the width of tissue cylinders is obtained from the relationship $N = \frac{n_C L_C}{V}$, where capillary density $N = 500/\text{mm}^2$. In model simulations, the total volume is conserved despite increases in vessel diameter or capillary number.

Oxygen saturation ($S(x)$) is obtained by equating the oxygen flux through a single vessel cross section with the rate of oxygen consumption per vessel length (q)

$$\frac{d}{dx}\left[Qc_0H_D S(x)\right] = -q, \quad (9)$$

where c_0 is the oxygen carrying capacity of red blood cells at 100% saturation and H_D is the discharge hematocrit.[19] Oxygen consumption per unit vessel length is defined as $q = \int_{r_i}^{r_i+d} M_0 2\pi r\,dr$, where M_0 is the (constant) level of oxygen demand in the tissue.

ATP concentration ($C(x)$) at position x is obtained using:

$$\frac{d}{dx}\left[\left(1-H_D\right)QC(x)\right] = \frac{\pi}{4}D^2H_T R\left[S(x)\right] - k_d\pi D\left(C(x) - C_{back}\right). \quad (10)$$

The first term on the right-hand side represents ATP release by red blood cells, where H_T is tube hematocrit and $R\left[S(x)\right]$ is the release rate of ATP. The release of ATP is a function of oxygen saturation since it has been observed that ATP is released at a greater rate under hypoxic conditions.[22] A linear fit for the oxygen saturation ($S(x)$) dependent release of ATP from[19] and[10] is used here.

$$R\left[S(x)\right] = R_0\left[1 - R_1 S(x)\right]. \quad (11)$$

In the second term of the right side of Equation 10, k_d is the ATP degradation rate constant. The rate of ATP degradation is proportional to the difference of the ATP concentration at a given point and a background level of ATP (C_{back}) assumed present in vessels under normoxic

conditions. Parameter values in the calculations for oxygen saturation and ATP concentration are taken directly from[10] and are provided in Table 2.

TABLE 1 Parameter values for vessel wall mechanics model

Parameter	COL	LA	SA
C_{pass}, dyn/cm	1773.1	933.1	403.8
C'_{pass}	8.293	8.293	10.88
C_{act}, dyn/cm	2075.19	1596.3	564.7
C'_{act}	0.7484	0.6804	0.7373
C''_{act}	0.2905	0.2905	0.3665
C_{myo}, cm/dyn	0.0101	0.0101	0.0226
C_{shear}, cm^2/dyn	0.0258	0.0258	0.0258
C_{meta}, 1/μM/cm	30	30	30
D_0, μm	266.03	140.00	60.59
C''_{tone}	4.783	13.31	19.39

2.1.2 | Chronic response: Arteriogenesis

Sustained dilation of the collateral artery and arterioles due to major arterial occlusion is assumed to trigger structural adaptation of these vessels.[23–25] In the model, structural enlargement is assumed to occur on a chronic time scale and is represented by the chronic diameter variable $(D_{chronic,i})$. Changes in the chronic diameter $(D_{chronic,i})$ are given by

$$\frac{dD_{chronic,i}}{dt} = k_0 \left(D_{acute,i} - D_{chronic,i}\right), \tag{12}$$

where k_0 is the time scale governing chronic vessel diameter dynamics.

As vessels undergo structural adaptation in the form of outward remodeling, the passive diameter of the vessels is also assumed to increase. Here, passive diameters are modeled as a saturating function of the slow-changing, chronic diameter $(D_{chronic,i})$

TABLE 2 Parameter values for oxygen transport, ATP release, conducted response, and differential equations

Description	Parameter	Value	Unit
Oxygen capacity of RBCs	c_0	0.5	cm^3 O_2/cm^3
Discharge hematocrit	H_D	0.4	
Oxygen demand	M_0	1–20	cm^3 O_2/100 cm^3/min
Tube hematocrit	H_T	0.3	
Rate of ATP degradation	k_d	2×10^{-4}	cm/s
Background level of ATP	C_{back}	0.5	μM
Initial saturation	$S(0)$	0.97	
Initial ATP concentration	$C(0)$	0.5	μM
Maximal rate of ATP release	R_0	1.234	nmol/cm^3/s
Effect of $S(x)$ on ATP release	R_1	1.026	
Length constant for S_{CR}	L_0	1	cm
Endpoint for S_{CR}	x_{end}	6.016	cm
Bifurcation point for S_{CR}	x_{bif}	2	cm
COL midpoint	x_{COL}	1	cm
LA midpoint	x_{LA}	2.571	cm
SA midpoint	x_{SA}	3.542	cm
Time constant for acute diameter	τ_d	1	s
Time constant for activation	τ_a	60	s
Time constant for chronic diameter	k_0	2.2×10^{-6}	s
Growth rate of passive diameter	β	1.3	
COL $D_{0,chronic}$ growth constant	η_{COL}	42.31	μm
LA $D_{0,chronic}$ growth constant	η_{LA}	19.94	μm
SA $D_{0,chronic}$ growth constant	η_{SA}	6.498	μm
Rate of angiogenesis	k_N	9×10^{-6}	s
Maximum number of capillaries	N_{max}	2.9×10^6	capillaries
Critical oxygen saturation	S_{crit}	0.33	

$$D_{0,\text{chronic},i}(t) = \frac{\beta D_{0,i} D_{\text{chronic},i}(t)}{\eta_i + D_{\text{chronic},i}(t)}, \quad (13)$$

where $D_{0,i}$ is the constant parameter value of passive diameter in the COL, LA, and SA used in the acute model.[10] Assuming control state values of oxygen demand and arterial pressure (see Section 2.2), the value $\beta = 1.3$ is chosen to yield a maximum passive collateral diameter of ~300 μm following occlusion.[7] η_i is chosen so that $D_{0,\text{chronic},i}(0) = D_{0,i}$.

2.1.3 | Chronic response: Angiogenesis

Angiogenesis is assumed to depend on the oxygen saturation at the end of the capillary compartment ($S_{\text{cap,end}}$). When oxygen saturation drops below a critical level (S_{crit}), the number of capillaries increases according to:

$$\frac{dN}{dt} = k_N \left(1 - \frac{N}{N_{\max}}\right) \max\left(S_{\text{crit}} - S_{\text{cap,end}}, 0\right) N, \quad (14)$$

where k_N is a constant that governs the rate of angiogenesis. The term $\left(1 - \frac{N}{N_{\max}}\right)$ limits the growth of new capillaries as total number of capillaries (N) approaches its maximum ($N_{\max}$). The maximum number of capillaries is chosen to be 1.7 times the number present in the control state since Jacobi et al.[26] observed around a 70% increase in the capillary density after femoral artery ligation and Chalothorn et al.[27] measured a 71% increase in capillary density three weeks after femoral ligation. In a computational study of VEGF gradients in PAD, Ji et al.[28] modeled the secretion of VEGF as a piecewise function of PO_2, assuming that VEGF was secreted at a basal rate under well-oxygenated conditions but that VEGF secretion increased once PO_2 dropped below 20 mmHg. Although VEGF is not explicitly modeled here, the critical oxygen saturation triggering angiogenesis is defined as $S_{\text{crit}} = 0.33$, which corresponds to a PO_2 of 20 mmHg. Parameter values for the wall mechanics model are given in Table 2; shaded rows show parameters taken from the acute model in[10] and non-shaded rows are parameters added for the chronic portion of the model.

2.2 | Control state and model simulations

A control (reference) state is defined to represent vascular conditions at a moderate activity level ($M_0 = 8.28$ cm^3 O_2/100 cm^3/min) and no occlusion. The control state value of the Krogh tissue cylinder width is 17.5 μm. Pressure entering the network from the aorta (P_a) is set to 140 mmHg in the control state, which corresponds to the mean arterial pressure in rats measured by Ziegler et al.[5] Venous pressure at the end of the calf (P_v) is assumed to be zero. As defined in[9] and,[10] $P_1 = 0.96\,P_a$, $P_{\text{distal}} = 0.90\,P_a$, and $P_2 = 0.93\,P_a$. P_3 and P_4 are chosen to be 75% and 28% of femoral pressure, respectively, based on pressure values in pre-capillary arterioles reported by Bohlen et al.[29]

The diameter of the CIA is set to 1109 μm based on the average of reported measurements,[30–32] and the diameters of the IIA and EF compartment are assumed to be 511 and 550 μm, respectively. Capillary diameter is assumed to be 8 μm. The assumed constant diameter and pressure drop along the CIA leads to a prescribed incoming flux for the system in the control state.

Control state activation is assumed to be 50% ($A = 0.5$) in the LA and SA and 99% ($A = 0.99$) in the collateral since there is little to no flow through collateral arteries in the absence of occlusion. C''_{tone} is chosen to satisfy the condition that $A = 0.5$ (LA, SA) and 0.99 (COL) in the control state. Given these assumptions, Equation 1 is reduced to a decoupled system of three equations that are solved for the control state values of D_{COL}, D_{LA}, and D_{SA}.

As in,[10,19] symmetry of vessel number and length in corresponding arteriolar and venular compartments of the calf microcirculation is assumed: $n_{\text{LA}} = n_{\text{LV}}$, $n_{\text{SA}} = n_{\text{SV}}$, $L_{\text{LA}} = L_{\text{LV}}$, and $L_{\text{SA}} = L_{\text{SV}}$. The symmetry assumption allows for the calculation of D_{LV} and D_{SV}:

$$D_{\text{LV}} = \left(\frac{\mu_{\text{LV}}\tau_{\text{LA}}}{\mu_{\text{LA}}\tau_{\text{LV}}}\right)^{\frac{1}{3}} D_{\text{LA}}; D_{\text{SV}} = \left(\frac{\mu_{\text{SV}}\tau_{\text{SA}}}{\mu_{\text{SA}}\tau_{\text{SV}}}\right)^{\frac{1}{3}} D_{\text{SA}}, \quad (15)$$

where diameter-dependent viscosities of blood in the COL, LA, SA, and C compartments are calculated using empirically based relationships defined by Pries et al.[20]. Viscosities are held fixed at their control state values in all model simulations. Wall shear stress values are assumed to be $\tau_{\text{LA}} = \tau_{\text{SA}} = \tau_{\text{C}} = 55$ dyn/cm^2 and $\tau_{\text{LV}} = \tau_{\text{SV}} = 10$ dyn/cm^2.[10,19] The control state value of shear stress in the collateral is calculated as $\tau_{\text{COL}} = 9.87$ dyn/cm^2.

Blood flow (Q) through the vessels in the LA, SA, and C compartments is calculated from $\tau = 32\mu Q/\pi D^3$. To obtain an equal flow split to the calf and thigh as observed experimentally,[8,33] the number of capillaries in the calf region is set to $n_c = 1.7 \times 10^6$. The total blood flow in the calf is given by $n_c Q_c$, and the numbers of large and small arterioles are determined using flow conservation: $n_c Q_c = n_{\text{SA}} Q_{\text{SA}} = n_{\text{LA}} Q_{\text{LA}}$. The CIA, IIA, EF, and COL compartments are assumed to each contain only one vessel.

Equating the lengths of symmetric compartments,[19] the pressure drop across the LV is calculated as:

$$\Delta P_{\text{LV}} = \left(\frac{\mu_{\text{LA}}}{\mu_{\text{LV}}}\right)^{\frac{1}{3}} \left(\frac{\tau_{\text{LV}}}{\tau_{\text{LA}}}\right)^{\frac{4}{3}} \Delta P_{\text{LA}}, \quad (16)$$

and similarly for ΔP_{SV}. These pressure drop values are used to calculate P_5 and P_6. The lengths of the CIA and collateral are assumed to be 7 and 2 cm, respectively. The remaining vessel lengths are calculated using Poiseuille's Law. A listing of all control state values is in.[10]

Vascular network dynamics in response to varying activity levels (oxygen demand) and incoming pressures (P_a) are simulated in both non-occluded and occluded conditions. To simulate a complete occlusion of the femoral artery, the diameter of the EF compartment is set to zero, causing its resistance to be effectively infinite. As a result, there is no blood flow through the EF branch and flow reaching the calf is solely supplied by the collateral vessel.

3 | RESULTS

Figure 2 shows the model-predicted values for acute diameter, chronic diameter, and activation of the collateral, LA and SA in both the occluded and non-occluded cases for a moderate value of oxygen demand (M_0 = 8.28 cm^3 O_2/100 cm^3/min). As expected, the steady-state diameter following occlusion (blue) is much higher than in the non-occluded (ie, control) state (black). In the collateral artery, activation approaches zero, indicating complete vasodilation (acute response); arteriolar enlargement due to structural adaptation (chronic response) is also predicted. In the LA and SA, a non-monotonic trend in activation levels with time leads to a low but nonzero activation, indicating that the natural compensatory response does not require complete dilation of all resistance vessels in the long run.

Changes in total calf blood flow for 30 days post-occlusion are depicted in Figure 3, assuming a moderate value of oxygen demand (M_0 = 8.28 cm^3 O_2/100 cm^3/min). Model predictions are compared with experimental data from studies of femoral artery occlusion in the rat.[8,33–40] The red dashed curve (labeled "Acute only") represents the effects of only the acute responses (ie, changes in activation due to pressure, shear stress, and metabolic responses while assuming a constant value for the chronic and passive diameters of the vessels). The blue curve (labeled "Full") depicts the level of flow restored when including both acute responses and chronic responses (arteriogenesis and angiogenesis). The responses are shown on an acute time frame in panel B. Following a significant drop in calf blood flow due to occlusion, the responses are very rapid (on the order of minutes) but are limited in their ability to restore flow. The amount of flow attained with acute responses only and the full model are practically

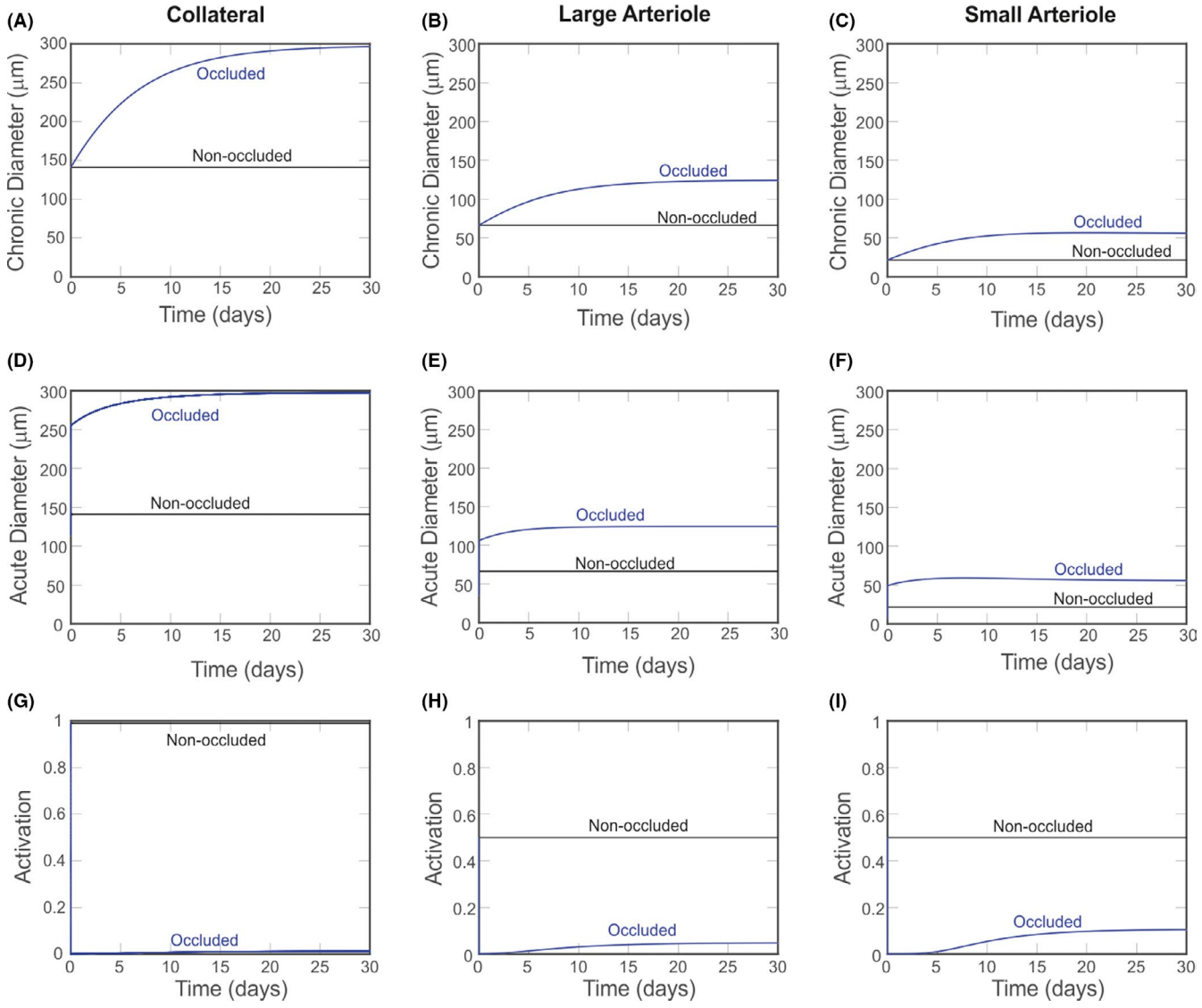

FIGURE 2 Changes in chronic diameters (A, B, C), acute diameters (D, E, F), and activation (G, H, I) in the collateral artery (first column), large arterioles (second column), and small arterioles (third column) in occluded (blue) and non-occluded (black) states for a moderate value of oxygen demand (M_0 = 8.28 cm^3 O_2/100 cm^3/min)

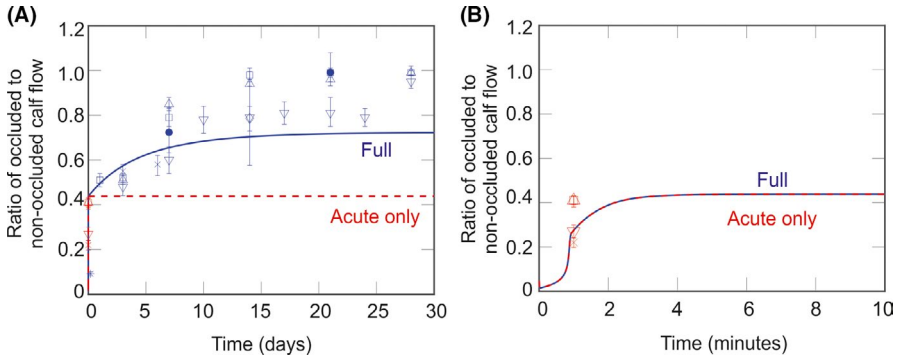

FIGURE 3 (A) Ratio of occluded to non-occluded blood flow in the calf with only acute vascular responses (dashed red) and with the combination of acute and chronic responses (blue). Data points are taken from: * Yang et al.,[33] • Paskins-Hurlburt and Hollenberg,[35] x Brouwers et al.,[36] □ Duan et al.,[37] ◇ Hirata et al.,[38] △ Duan et al.,[39] ▽ Tang et al.,[40] (B) A zoomed in version of panel (A) to depict the fast time scale of the acute response (order of minutes)

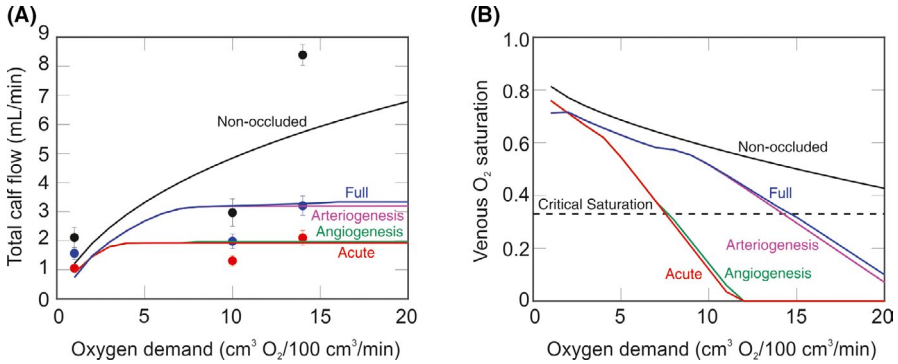

FIGURE 4 (A) Total calf blood flow with varying levels of oxygen demand in non-occluded (black) and occluded cases given the following responses: acute responses only (red), angiogenesis with acute responses (green), arteriogenesis with acute responses (magenta), and all chronic responses combined with acute responses (blue). Data points are taken from Ziegler et al.[5] and correspond to flow data with no occlusion (black circles), flow data following acute clamping of the femoral artery (red circles), and flow data from two weeks after chronic ligation of the femoral artery (blue circles). (B) Venous oxygen saturation as oxygen demand is varied. Non-occluded and occluded simulations are as in panel (B). The black dashed line indicates the critical saturation level ($S_{crit} = 0.33$) that triggers angiogenesis (see Equation 14)

identical during this time since it is too early for chronic responses to fully take effect. Figure 3A indicates that the coupling of acute and chronic responses allows for further flow compensation, even though flow is never fully restored to its non-occluded level.

Steady-state values of total calf blood flow for varying levels of oxygen demand are given in Figure 4A. The black curve represents flow in the non-occluded state. The remaining curves depict flow levels in the occluded state. The red curve shows the flow results when only acute responses are simulated. Green, magenta, and blue curves show predicted flows when angiogenesis, arteriogenesis, or both of these chronic responses are added to the acute response, respectively. The data points are taken from Ziegler et al.[5] which measured femoral venous outflow in WKY rats during normal conditions (black circles), acute clamping of the femoral artery (red circles), and chronic ligation for 2 weeks (blue circles). Electrical stimulation of the calf muscle was used to simulate increased activity levels,[5] corresponding to varied levels of oxygen demand. The frequencies of electrical stimulation were converted to approximate corresponding levels of oxygen demand in cm^3 O_2/100 cm^3/min as in.[10]

In the non-occluded case (black curve), the model predictions and experimental data indicate that blood flow increases to meet increasing levels of oxygen demand. However, following occlusion, calf blood flow fails to increase beyond a certain level despite further increases in demand. If only acute responses are present (red curve), this maximum is reached for an oxygen demand of 4 cm^3 O_2/100 cm^3/min. Nearly an identical trend is observed with the addition of angiogenesis (green). In contrast, the addition of arteriogenesis (magenta) results in a more noticeable increase in flow and delays the value of oxygen demand at which flow reaches its maximum to 7 cm^3 O_2/100 cm^3/min. Although minimal, the effect of angiogenesis is slightly greater when arteriogenesis is present than when it is absent. Regardless, in the presence of all acute and chronic responses, total calf blood flow remains below non-occluded levels, especially as oxygen demand is increased.

Figure 4B shows the predicted level of venous oxygen saturation as oxygen demand is increased from 1 to 20 cm^3 O_2/100 cm^3/min with the same responses isolated as in panel A. The dashed horizontal line denotes the critical saturation below which angiogenesis is

assumed to occur. In the non-occluded case, oxygen saturation stays above this critical level for all values of oxygen demand. Following occlusion, oxygen saturation falls below the critical level in all cases and approaches zero when only acute responses or acute responses combined with angiogenesis are assumed. The inclusion of arteriogenesis prevents oxygen saturation from falling to zero for the values of oxygen demand considered.

The effects of occlusion on blood flow autoregulation are examined in Figure 5. In Figure 5A, the model-predicted values of total blood flow in the calf when varying arterial pressure are compared with experimental data from Paskins-Hurlburt and Hollenberg.[35] Autoregulation is a phenomenon in which flow remains relatively constant despite changes in intraluminal pressure. In the absence of autoregulation, flow would increase passively with pressure. In the non-occluded case (black curve), an autoregulation plateau is predicted for pressures of about 50–200 mmHg. This autoregulation plateau is shifted dramatically following occlusion. In particular, a plateau is observed for pressures between 220 and 270 mmHg when only acute responses are present (red). The addition of chronic responses (blue) reduces this drastic shift in autoregulation to pressures between 155 and 205 mmHg. For pressure ranges of length 100 mmHg, an autoregulation ratio is defined for these three cases as the ratio of flow at the higher pressure (Q_2) of the plateau to flow at the lower pressure of the plateau (Q_1). In the non-occluded case, this ratio is approximately 1.25. In the occluded case, this ratio is increased to 5.72. However, these ratios return to about 1.25–1.29 when accounting for the shift in the autoregulation curves to higher pressures following occlusion. Table 3 provides a summary of these autoregulation ratios for the cases depicted in Figure 5A.

Figure 5B–D depicts the steady-state diameters of the COL, LA, and SA as the incoming pressure to the system (P_a), is increased. In the non-occluded case (black curve), all three vessel diameters decrease over the range of pressures corresponding to the autoregulation plateau. Following occlusion, LA and SA diameters constrict over the shifted autoregulation pressure range, but COL diameters are predicted to increase.

Figure 6 depicts the impact of the individual mechanisms underlying the acute response. Mechanisms are turned "off" by setting the corresponding component of S_{tone} to its value in the control state and requiring it to remain at this value despite changes in local stimuli. In the non-occluded case (Figure 6A), the ability of the vasculature to autoregulate is maintained if either the metabolic (green curve) or myogenic (blue) responses are active. As seen in,[10] combining the COL shear and LA and SA metabolic responses (gray) produces the same result as having only the metabolic response. If only the shear response in all compartments (magenta) or the metabolic response in the collateral (black) are activated, flow autoregulation is not predicted.

A similar trend is observed in Figure 6B for the occluded case. As in the non-occluded case, there is no autoregulation if just the shear responses (magenta) or the COL metabolic response (red) are present. In the other occluded scenarios (blue, green, gray, black), the autoregulation curves shift significantly toward higher pressures. In some cases, small pressure ranges with sharp increases in blood flow are observed. The pressures at which these drastic changes occur depend upon the initial conditions, indicating that there are regions of bistability in these cases. If pressure is incrementally increased from the control value (140 mmHg) instead of decreased

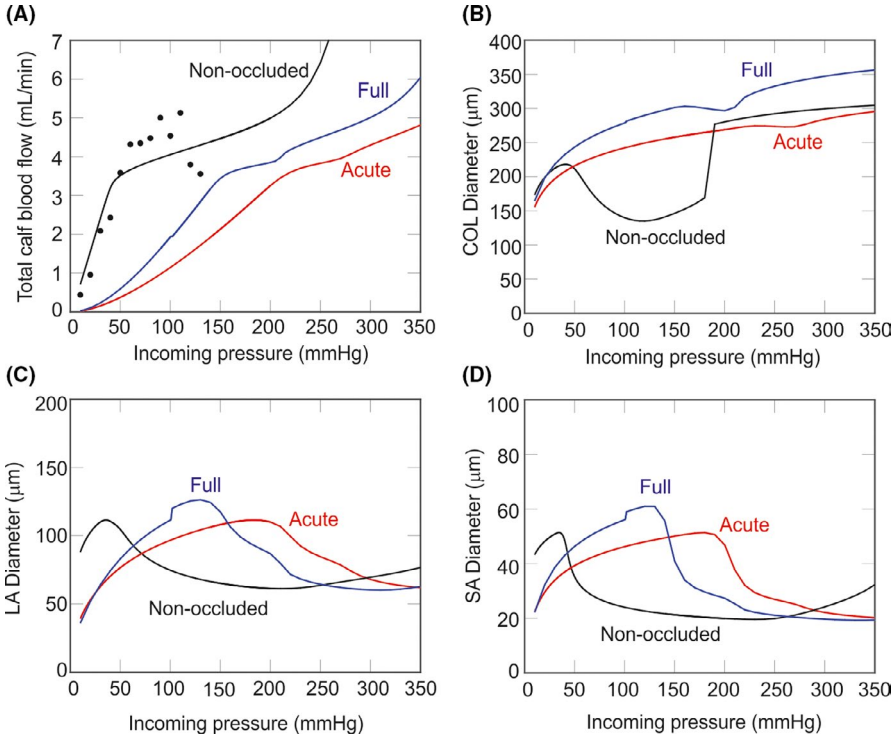

FIGURE 5 (A) Total blood flow in the calf (collateral-dependent region) as incoming arterial pressure (P_a) is increased with no occlusion (black), occlusion with acute responses only (red), and occlusion with acute and chronic responses (blue). Data points for non-occluded conditions are obtained from Paskins-Hurlburt and Hollenberg.[35] (B–D). Steady-state diameters as incoming arterial pressure (P_a) is varied in the collateral (panel B), large arteriole (panel C), and small arteriole (panel B), response colors as in panel A

TABLE 3 Ordered pairs of arterial pressure (mmHg) and the corresponding total calf blood flow (ml/min). The autoregulation ratio in the third column is obtained by dividing flow at the second point (P_{a2}, Q_2) by flow at the first point (P_{a1}, Q_1)

Case	(P_{a1}, Q_1)	(P_{a2}, Q_2)	Ratio $\frac{Q_2}{Q_1}$
Non-occluded	(50, 3.587)	(150, 4.468)	1.2456
Occluded, acute	(50, 0.373)	(150, 2.133)	5.7185
	(220, 3.602)	(320, 4.504)	1.2504
Occluded, full	(50, 0.5916)	(150, 3.443)	5.8198
	(155, 3.532)	(255, 4.543)	1.2862

from 400 mmHg, these disruptions in the pressure-flow curve occur at higher pressure values (not shown).

4 | DISCUSSION

The present study models compensatory responses to femoral arterial occlusion in the rat hindlimb by coupling the chronic processes of angiogenesis and arteriogenesis to a model of acute responses which regulate smooth muscle tone. The model results show that resistance vessels fully dilate on acute time scales but exhibit nonzero activation on a chronic time scale; the collateral artery, however, increases in diameter on both acute and chronic time frames and remains fully dilated. Although the arterioles have the potential to dilate further, an intervention that induces total dilation of the arterioles is unlikely to have a significant impact on total blood flow to the calf since the incoming flux to the calf is determined by the flow through the collateral.

The model also reveals that arteriogenesis, not angiogenesis, is primarily responsible for the improvements in calf blood flow observed with the addition of chronic responses. Coupling angiogenesis with arteriogenesis provides only a small improvement over arteriogenesis. Arteriogenesis is likely more effective in enhancing blood flow and oxygen saturation because it allows larger vessels to attain higher diameters and thus significantly decreases vascular resistance. In addition, arteriogenesis affects the collateral, which is the upstream vessel responsible for redirecting blood flow to the calf after occlusion. Meanwhile, by adding vessels to the capillary compartment, angiogenesis only slightly lowers the overall resistance.

When only acute responses to occlusion are considered, blood flow compensation quickly attains a maximum because the COL, LA, and SA all dilate completely. With the addition of chronic responses, blood flow continues to increase, although it plateaus before 30 days. This observation indicates that while angiogenesis and arteriogenesis are important components of flow compensation, they are not sufficient to restore flow to non-occluded levels, suggesting the need for additional intervention. Exercise training has been shown to enhance the structural enlargement of collateral vessels after femoral artery occlusion in rats[8] and could potentially provide the additional stimulus needed to bring flow to healthy levels. However, the effects of exercise training were not modeled in the present study.

Arterial occlusion also induces changes in the vasculature that cause the autoregulatory range of pressures to shift to significantly higher values. This shift in the autoregulation range immediately after occlusion may be difficult to observe in experiment since the range of 250–350 mmHg is much higher than normal physiological arterial pressures. The inclusion of chronic responses works to bring the autoregulatory pressure range closer to the non-occluded range, which is consistent with the study by Paskins-Hurlburt and Hollenberg that showed that the pressure-flow relationship of collateral vessels becomes closer to normal after longer periods of time post-occlusion.[35]

The dependence of the autoregulation curves on the history of the system (see bistability discussion for Figure 6B) indicates that responses to occlusion may depend on the previous health and conditions of the vasculature. In the non-occluded case, the addition of the shear response in the collateral compartment has little to no effect on autoregulation. After occlusion, the inclusion of the shear response in the collateral compartment is necessary whereas the metabolic response in the collateral does not impact the ability to autoregulate. Although the shear response in the collateral is insignificant in the non-occluded case, the increase in collateral blood flow and the resulting shear response is an essential component of flow compensation following occlusion.

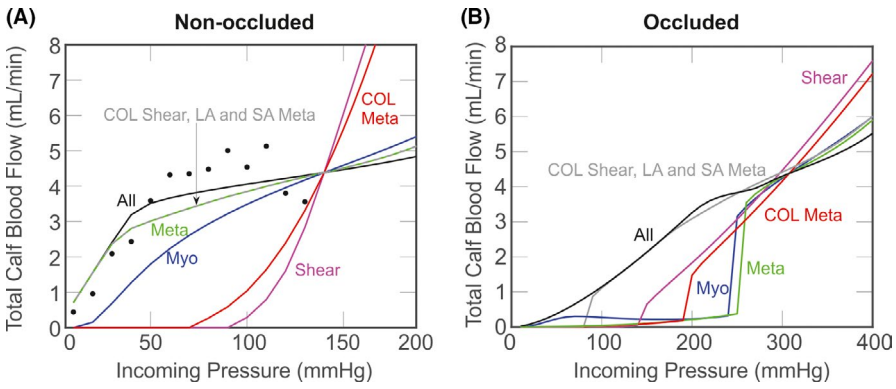

FIGURE 6 Total calf blood flow for varying levels of incoming pressure (P_a) as different acute response mechanisms are switched on or off. Data points (black circles) are obtained for the non-occluded case from Paskins-Hurlburt and Hollenberg.[35] (A) Non-occluded case. (B) Occluded case

As with any mathematical model, simplifying assumptions were made in this study to model both acute and chronic responses in the vascular network after femoral arterial occlusion. Vessels within a single compartment are assumed identical even though, in reality, vessels of the same type may vary in length and tortuosity. In addition, the conducted metabolic signal in this study was based on the release of ATP by red blood cells, although a wall-derived conducted response signal independent of red blood cells has also been shown in other models to lead to improved oxygen transport predictions in heterogeneous networks which have unequal partitioning of hematocrit at bifurcations.[41] However, since the present vascular network is homogeneous, use of an ATP-derived signal is justified. Additional mechanisms besides pressure, shear stress, and metabolic demand may contribute to the modulation of vascular tone, such as the effects of the nervous system on smooth muscle tone,[42] but these were not explicitly modeled here. The chronic responses in the model are not fully mechanistic; arteriogenesis is assumed to occur due to sustained vasodilation, and angiogenesis depends directly on oxygen saturation levels. These assumptions are reasonable since the mechanisms that lead to structural enlargement are thought to be similar to those that induce vasodilation,[23–25] and factors driving angiogenesis, such as vascular endothelial growth factor (VEGF), are released in response to hypoxia.[43,44] Incorporating more specific mechanisms into the equations for arteriogenesis and angiogenesis is a goal of future modeling work.

Simulations of both the acute and chronic time frames used a constant value of oxygen demand (M_0). The physiological interpretation of oxygen demand in the acute case is the activity level, which ranges from rest (low oxygen demand) to intense exercise (high demand). However, this is more difficult to interpret in the chronic case because individuals typically do not remain at a constant activity level for long periods of time. Nevertheless, the model predictions for high oxygen demand values are useful in predicting an upper bound of blood flow levels attained when coupling acute and chronic responses. Following occlusion, chronic responses are predicted to restore the vasculature closer to its healthy, non-occluded state primarily due to the predominant effects of collateral arteriogenesis. As a result, treatments for PAD that augment the structural enlargement of collateral vessels may be more beneficial than those that promote angiogenesis.

5 | PERSPECTIVES

The model suggests that arteriogenesis is primarily responsible for the improvements in blood flow compensation observed with the addition of chronic responses, and that the role of angiogenesis is minimal in comparison. Furthermore, the model predicts that in addition to reducing blood flow to the distal region, arterial occlusion also impairs vessel autoregulation in this region. Therefore, effective treatments for PAD should promote collateral arteriogenesis with the goal of restoring both normal blood flow levels and autoregulatory abilities.

DATA AVAILABILITY STATEMENT

The data that support the findings of this study are available from the corresponding author upon reasonable request.

ORCID

Jared Barber https://orcid.org/0000-0002-8414-6642
Chandan K. Sen https://orcid.org/0000-0003-3151-5202
Julia Arciero https://orcid.org/0000-0002-2882-3653

REFERENCES

1. Hirsch AT, Criqui MH, Treat-Jacobson D, et al. Peripheral arterial disease detection, awareness, and treatment in primary care. *JAMA*. 2001;286(11):1317-1324.
2. Ouriel K. Peripheral arterial disease. *Lancet*. 2001;358(9289):1257-1264.
3. Helisch A, Schaper W. Arteriogenesis: the development and growth of collateral arteries. *Microcirculation*. 2003;10(1):83-97.
4. Unthank JL, Nixon JC, Lash JM. Early adaptations in collateral and microvascular resistances after ligation of the rat femoral artery. *J Appl Physiol*. 1995;79(1):73-82.
5. Ziegler MA, DiStasi MR, Miller SJ, Dalsing MC, Unthank JL. Novel method to assess arterial insufficiency in rodent hind limb. *J Surg Res*. 2016;201(1):170-180.
6. Chalothorn D, Clayton JA, Zhang H, Pomp D, Faber JE. Collateral density, remodeling, and VEGF-A expression differ widely between mouse strains. *Physiol Genomics*. 2007;30(2):179-191.
7. Herzog S, Sager H, Khmelevski E, Deylig A, Ito WD. Collateral arteries grow from preexisting anastomoses in the rat hindlimb. *Am J Physiol Heart Circ Physiol*. 2002;283(5):H2012-H2020.
8. Prior BM, Lloyd PG, Ren J, et al. Time course of changes in collateral blood flow and isolated vessel size and gene expression after femoral artery occlusion in rats. *Am J Physiol Heart Circ Physiol*. 2004;287(6):H2434-H2447.
9. Arciero J, Lembcke L, Burch M, Franko E, Unthank J. Assessing the hemodynamic contribution of capillaries, arterioles, and collateral arteries to vascular adaptations in arterial insufficiency. *Microcirculation*. 2020;27(2):e12591.
10. Zhao E, Barber J, Burch M, Unthank J, Arciero J. Modeling acute blood flow responses to a major arterial occlusion. *Microcirculation*. 2020;27(4):e12610.
11. Pries AR, Reglin B, Secomb TW. Structural adaptation of microvascular networks: functional roles of adaptive responses. *Am J Physiol Heart Circ Physiol*. 2001;281(3):H1015-H1025.
12. Pries AR, Secomb TW, Gaehtgens P. Structural adaptation and stability of microvascular networks: theory and simulations. *Am J Physiol*. 1998;275(2):H349-H360.
13. Gruionu G, Hoying JB, Gruionu LG, Laughlin MH, Secomb TW. Structural adaptation increases predicted perfusion capacity after vessel obstruction in arteriolar arcade network of pig skeletal muscle. *Am J Physiol Heart Circ Physiol*. 2005;288(6):H2778-H2784.
14. Gruionu G, Hoying JB, Pries AR, Secomb TW. Structural remodeling of mouse gracilis artery after chronic alteration in blood supply. *Am J Physiol Heart Circ Physiol*. 2005;288(5):H2047-H2054.
15. Ji JW, Tsoukias NM, Goldman D, Popel AS. A computational model of oxygen transport in skeletal muscle for sprouting and splitting modes of angiogenesis. *J Theor Biol*. 2006;241(1):94-108.
16. Liu G, Qutub AA, Vempati P, Gabhann FM, Popel AS. Module-based multiscale simulation of angiogenesis in skeletal muscle. *Theor Biol Med Model*. 2011;8:6.

17. Secomb TW, Alberding JP, Hsu R, Dewhirst MW, Pries AR. Angiogenesis: an adaptive dynamic biological patterning problem. *PLoS Comput Biol*. 2013;9(3):e1002983.
18. Carlson BE, Arciero JC, Secomb TW. Theoretical model of blood flow autoregulation: roles of myogenic, shear-dependent, and metabolic responses. *Am J Physiol Heart Circ Physiol*. 2008;295(4):H1572-H1579.
19. Arciero JC, Carlson BE, Secomb TW. Theoretical model of metabolic blood flow regulation: roles of ATP release by red blood cells and conducted responses. *Am J Physiol Heart Circ Physiol*. 2008;295(4):H1562-H1571.
20. Pries AR, Secomb TW, Gaehtgens P, Gross JF. Blood flow in microvascular networks. Experiments and simulation. *Circ Res*. 1990;67(4):826-834.
21. Krogh A. The supply of oxygen to the tissues and the regulation of the capillary circulation. *J Physiol*. 1919;52(6):457-474.
22. Bergfeld GR, Forrester T. Release of ATP from human erythrocytes in response to a brief period of hypoxia and hypercapnia. *Cardiovasc Res*. 1992;26(1):40-47.
23. Hoefer IE, den Adel B, Daemen MJ. Biomechanical factors as triggers of vascular growth. *Cardiovasc Res*. 2013;99(2):276-283.
24. Skalak TC, Price RJ. The role of mechanical stresses in microvascular remodeling. *Microcirculation*. 1996;3(2):143-165.
25. Unthank JL, Nixon JC, Burkhart HM, Fath SW, Dalsing MC. Early collateral and microvascular adaptations to intestinal artery occlusion in rat. *Am J Physiol*. 1996;271(3 Pt 2):H914-H923.
26. Jacobi J, Porst M, Cordasic N, et al. Subtotal nephrectomy impairs ischemia-induced angiogenesis and hindlimb re-perfusion in rats. *Kidney Int*. 2006;69(11):2013-2021.
27. Chalothorn D, Zhang H, Clayton JA, Thomas SA, Faber JE. Catecholamines augment collateral vessel growth and angiogenesis in hindlimb ischemia. *Am J Physiol Heart Circ Physiol*. 2005;289(2):H947-H959.
28. Ji JW, Mac Gabhann F, Popel AS. Skeletal muscle VEGF gradients in peripheral arterial disease: simulations of rest and exercise. *Am J Physiol Heart Circ Physiol*. 2007;293(6):H3740-H3749.
29. Bohlen HG, Gore RW, Hutchins PM. Comparison of microvascular pressures in normal and spontaneously hypertensive rats. *Microvasc Res*. 1977;13(1):125-130.
30. Gabeler EE, van Hillegersberg R, van Eps RGS, et al. A comparison of balloon injury models of endovascular lesions in rat arteries. *BMC Cardiovasc Disord*. 2002;2:16.
31. Karwowski JK, Markezich A, Whitson J, Abbruzzese TA, Zarins CK, Dalman RL. Dose-dependent limitation of arterial enlargement by the matrix metalloproteinase inhibitor RS-113,456. *J Surg Res*. 1999;87(1):122-129.
32. Abbruzzese TA, Guzman RJ, Martin RL, Yee C, Zarins CK, Dalman RL. Matrix metalloproteinase inhibition limits arterial enlargements in a rodent arteriovenous fistula model. *Surgery*. 1998;124(2):328–334; discussion 334–5.
33. Yang HT, Laughlin MH, Terjung RL. Prior exercise training increases collateral-dependent blood flow in rats after acute femoral artery occlusion. *Am J Physiol Heart Circ Physiol*. 2000;279(4):H1890-H1897.
34. Leong-Poi H, Christiansen J, Heppner P, et al. Assessment of endogenous and therapeutic arteriogenesis by contrast ultrasound molecular imaging of integrin expression. *Circulation*. 2005;111(24):3248-3254.
35. Paskins-Hurlburt AJ, Hollenberg NK. "Tissue need" and limb collateral arterial growth. Skeletal contractile power and perfusion during collateral development in the rat. *Circ Res*. 1992;70(3):546-553.
36. Brouwers O, Yu L, Niessen P, et al. Glyoxalase-1 overexpression partially prevents diabetes-induced impaired arteriogenesis in a rat hindlimb ligation model. *Glycoconj J*. 2016;33(4):627-630.
37. Duan J, Murohara T, Ikeda H, et al. Hyperhomocysteinemia impairs angiogenesis in response to hindlimb ischemia. *Arterioscler Thromb Vasc Biol*. 2000;20(12):2579-2585.
38. Hirata K, Li T-S, Nishida M, et al. Autologous bone marrow cell implantation as therapeutic angiogenesis for ischemic hindlimb in diabetic rat model. *Am J Physiol Heart Circ Physiol*. 2003;284(1):H66-H70.
39. Duan J, Murohara T, Ikeda H,, et al. Hypercholesterolemia inhibits angiogenesis in response to hindlimb ischemia: nitric oxide-dependent mechanism. *Circulation*. 2000;102(19 Suppl 3):III-370-III-376.
40. Tang GL, Chang DS, Sarkar R, Wang R, Messina LM. The effect of gradual or acute arterial occlusion on skeletal muscle blood flow, arteriogenesis, and inflammation in rat hindlimb ischemia. *J Vasc Surg*. 2005;41(2):312-320.
41. Roy TK, Pries AR, Secomb TW. Theoretical comparison of wall-derived and erythrocyte-derived mechanisms for metabolic flow regulation in heterogeneous microvascular networks. *Am J Physiol Heart Circ Physiol*. 2012;302(10):H1945-H1952.
42. Folkow B. Role of the nervous system in the control of vascular tone. *Circulation*. 1960;21:760-768.
43. Hershey JC, Baskin EP, Glass JD, et al. Revascularization in the rabbit hindlimb: dissociation between capillary sprouting and arteriogenesis. *Cardiovasc Res*. 2001;49(3):618-625.
44. Shweiki D, Itin A, Soffer D, Keshet E. Vascular endothelial growth factor induced by hypoxia may mediate hypoxia-initiated angiogenesis. *Nature*. 1992;359(6398):843-845.

How to cite this article: Zhao E, Barber J, Sen CK, Arciero J. Modeling acute and chronic vascular responses to a major arterial occlusion. *Microcirculation*. 2022;29:e12738. doi:10.1111/micc.12738